Unsteady flow through *in-vitro* models of the glottis

G. C. J. Hofmans and G. Groot
Fluid Dynamics Laboratory, Faculty of Applied Physics, Eindhoven University of Technology, Postbus 513, 5600 MB Eindhoven, The Netherlands

M. Ranucci and G. Graziani
University "La Sapienza," Dipartimento Di Meccanica E Aeronautica, Via Eudossiana 18, 00184 Rome, Italy

A. Hirschberg[a)]
Fluid Dynamics Laboratory, Faculty of Applied Physics, Cascade 2.24, Eindhoven University of Technology, Postbus 513, 5600 MB Eindhoven, The Netherlands

(Received 20 August 2001; revised 13 November 2002; accepted 12 December 2002)

The unsteady two-dimensional flow through fixed rigid *in vitro* models of the glottis is studied in some detail to validate a more accurate model based on the prediction of boundary-layer separation. The study is restricted to the flow phenomena occurring within the glottis and does not include effects of vocal-fold movement on the flow. Pressure measurements have been carried out for a transient flow through a rigid scale model of the glottis. The rigid model with a fixed geometry driven by an unsteady pressure is used in order to achieve a high accuracy in the specification of the geometry of the glottis. The experimental study is focused on flow phenomena as they might occur in the glottis, such as the asymmetry of the flow due to the Coanda effect and the transition to turbulent flow. It was found that both effects need a relatively long time to establish themselves and are therefore unlikely to occur during the production of normal voiced speech when the glottis closes completely during part of the oscillation cycle. It is shown that when the flow is still laminar and symmetric the prediction of the boundary-layer model and the measurement of the pressure drop from the throat of the glottis to the exit of the glottis agree within 40%. Results of the boundary-layer model are compared with a two-dimensional vortex-blob method for viscous flow. The difference between the results of the simpified boundary-layer model and the experimental results is explained by an additional pressure difference between the separation point and the far field within the jet downstream of the separation point. The influence of the movement of the vocal folds on our conclusions is still unclear.
[DOI: 10.1121/1.1547459]

PACS numbers: 43.70.Bk [AL]

I. INTRODUCTION

Researchers in the field of biomechanics have been using numerical simulations as a useful tool for their studies. Topics that are related to the flow of blood through arteries received a lot of attention in recent years (Rosenfeld, 1995; Luo and Pedley, 1996; Pedrizzetti, 1996) [for an overview of recent work on this subject see Pedley and Luo (1998)]. Also the flow of air through the glottis has been the subject of numerical studies and experimental studies. Interest in this topic is motivated by two research aims: one is the development of prosthetic vocal folds (Lous *et al.*, 1998; De Vries, 2000) and the other is the development of artificial speech models. Recently some attempts at numerically simulating the flow through the glottis including forced vocal-fold movement have been carried out (Alipour and Titze, 1996; Alipour *et al.*, 1996). Also the effect of an asymmetry in the glottal channel on speech production has been investigated by means of steady pressure measurements along the glottal channel supported by numerical simulations (Scherer *et al.*, 2001). Although a complete simulation of the vocal-fold movement and the air flow through the glottis can yield some interesting results, it is not a solution to the problem of artificial (real-time) speech modeling in the near future.

One approach in speech modeling is to model the interaction of the air flow through the glottis and the movement of the vocal folds using simplified models. The problems that are encountered are numerous since the flow through the glottis is a result of the coupling between complex fluid dynamics and complex elastic structure (vocal folds) behavior. Usually both aspects are simplified until such a level is reached that artificial real-time speech production is possible. This leads to oversimplifying both aspects of vocal-fold movement but especially the fluid dynamical description has been reduced to a caricature of the actual flow. An important parameter in these flow models is the point at which the airflow separates from the vocal folds. This parameter determines not only the volume flow through the glottis but also the hydrodynamic forces exerted on the vocal folds.

In most models of the flow through the glottis *ad hoc* assumptions are made about the separation point in the glottis. The most well known model of this kind is the model of Ishizaka and Flanagan (1972) in which flow separation at

[a)]Author to whom correspondence should be addressed. Electronic mail: A.Hirschberg@phys.tue.nl

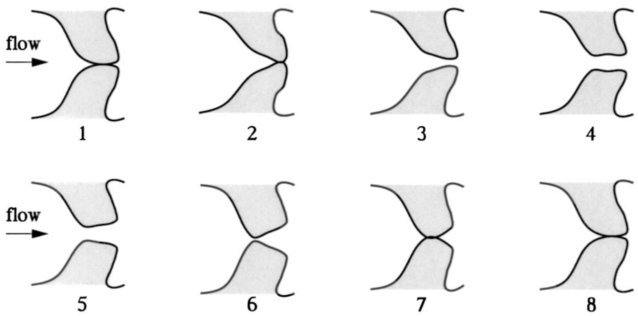

FIG. 1. Typical vocal-fold movement during one oscillation. Note the changing shape of the glottis.

sharp edges is assumed. Such sharp edges are of course not present in the glottis. An attempt was made to improve the description of flow separation within the glottis by using a quasi-steady model based on the boundary-layer theory (Pelorson *et al.*, 1994). It was shown that this improved the results obtained from a simplified mechanical model in which the vocal folds are each represented by two coupled oscillators. This approach is similar to a model proposed for collapsible tubes (Cancelli and Pedley, 1985). The results of this model together with an idea of Liljencrants (1993) formed the basis of a new model (Lous *et al.*, 1998). In the same paper the consequences of the various simplifying assumptions that are made in most models for the vocal-fold movement are also discussed. A discussion on the flow phenomena that might be important for a model of the flow through the glottis can be found in Hirschberg *et al.* (1996), while in Pelorson *et al.* (1997) the focus is on the fluid dynamics of so-called bilabial plosives.

In Fig. 1 a typical cycle of the vocal-fold movement is presented. Note the changing shape of the glottis due to the way in which the vocal folds open and close. Because pressure is applied upstream of the vocal folds, they first start to open at the upstream side (panels 2 and 3 in Fig. 1). This results in a converging glottis shape during the opening phase of the glottis. The closing of the glottis also starts at the upstream side, resulting in a diverging glottis shape during the closing phase (panels 5 and 6 in Fig. 1). Apparently the movement of the vocal-fold tissue at the downstream side is always lagging behind the movement at the upstream side. A glottal pulse that is the result of such a vocal-fold movement representing the sound /a/ at 110 Hz is sketched in Fig. 2 [after data measured by Rothenberg (1981)].

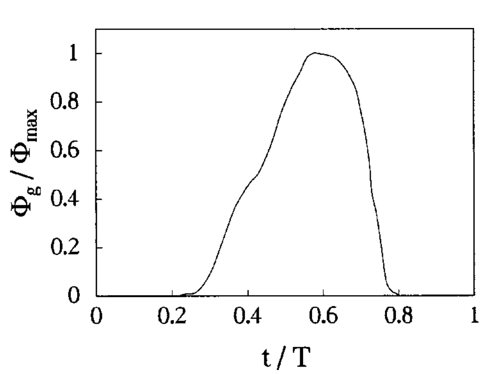

FIG. 2. Normalized glottal flux ϕ_g for the sound /a/ at 110 Hz.

In this paper we present an experimental, theoretical, and numerical study of the flow through *in vitro* models of the glottis. In order to limit ourselves to the fluid dynamical aspects of the flow we used rigid fixed (scale) models of the vocal folds. The size is approximately three times the size of the real vocal folds and the shape of these scale models is inspired by the typical shape of the glottis during the closing phase. In this phase the slowly diverging shape of the glottis implies a rather uncertain position of the separation point. This is the reason why we focus on this geometry. In the actual flow through the glottis an almost steady pressure difference is imposed across the vocal folds, while the opening and closing of the glottis result in an unsteady flow. We decided to use fixed models (not oscillating) for the sake of a high accuracy in the specification of the geometry of the model of the glottis. In order to maintain a similarity to the actual flow through the glottis, an unsteady pressure drop is imposed across the vocal folds. Care is taken that the nondimensional control parameters determining the flow through the glottis have the relevant values. In the glottis these parameters are the Strouhal number and the Reynolds number. The Strouhal number is defined as $\mathrm{Sr} = l/u_0T$ in which l is a stream-wise length scale of the glottis (5–10 mm), u_0 is a typical velocity in the glottis (10–30 m/s), and T is a typical time scale of the vocal-fold movement. For men a typical frequency of oscillation is 10^2 Hz, while for women it is twice as large at approximately 2×10^2 Hz. A better time scale is, however, the opening or closing time of the glottis (2–4 ms). The Reynolds number is defined as $\mathrm{Re} = h_0u_0/\nu$, in which h_0 is the typical height of the glottis (1–2 mm) and ν is kinematic viscosity of air ($\nu = 1.5\times10^{-5}\,\mathrm{m^2/s}$ at atmospheric pressure and room temperature). The Strouhal number (typically of order 10^{-1}) is a measure of the influence of unsteady effects on the flow, while the Reynolds number (typically of order 10^3) reflects the importance of viscous effects on the flow. Due to the geometrical scaling factor 3, when the Reynolds and Strouhal analogies are respected, the measured velocities should be multiplied by 3, the pressure should be multiplied by 9, and the time intervals should be divided by 9 in order to compare to physiological conditions. In our experiments Re is in the range of 2×10^3–8×10^3 corresponding to very loud speech. The Reynolds number is also an indication for the onset of turbulence. In the free jet at the exit of the glottis a Reynolds number above 2×10^3 implies turbulence. The turbulence in the glottis upstream of the separation point is however not expected because $\mathrm{Re}\cdot l/h_0 \leqslant 10^5 [l/h_0 = \mathcal{O}(10)]$. The Strouhal number in our experiments is of the order of magnitude of 10^{-1}.

In speech modeling the important quantity that has to be modeled accurately is the acoustic source that is the result of the vocal fold movement. This source is the unsteady volume flux through the glottis. In particular the time dependence of this flux during the closing phase of the vocal-fold movement is important because it contains most of the higher harmonics for which our hearing is most sensitive. This movement is driven by the pressure at the throat of the glottis. So, to evaluate the validity and accuracy of the simplified quasi-steady boundary-layer model, we compare the numeri-

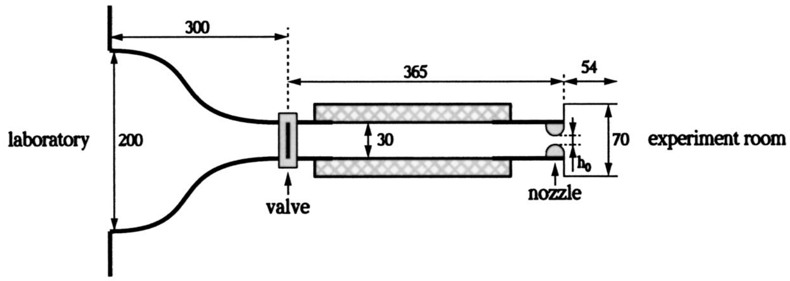

FIG. 3. Schematic representation of the experimental setup. Measures are in millimeters. h_0 is the (throat) height of the aperture (typically 1 or 3 mm). The shaded area represents the rubber foam padding on the inside of the upstream channel.

cally determined pressure at the throat to the theoretical prediction.

This paper has the following structure. We start by presenting some steady pressure measurements in a liplike round model and compare them to a simplified boundary-layer model. Next unsteady pressure measurements in both a liplike model and two diverging vocal-fold models are presented. Attention is paid to the various flow phenomena that are observed. Finally some results of numerical simulations of the flow through these models are presented. Both numerical and experimental results are compared to a quasi-steady boundary-layer model in order to study the applicability and accuracy of such a model in a description of the flow through the glottis.

II. EXPERIMENTS

A. Experimental setup

The experimental results that are presented in this paper have been obtained in the setup shown in Fig. 3. A sliding valve operated by a spring blade separates two large pressure reservoirs: laboratory (3500 m^3) and experiment room (75 m^3). A cylindrical pipe connects the inlet section to the glottis section. In order to damp mechanical and acoustic vibrations, the inner walls of this pipe are covered by a rubber foam (the shaded area in Fig. 3). The nozzle at the open pipe termination is a smooth constriction that is built out of either liplike round models or diffuser models that form a glottis-like channel. The brass blocks that form the geometry of the constriction are shown in Fig. 4. The block and hence the length of the glottal slit is 30 mm (i.e., the length in the third dimension not shown in the figure). All these blocks can be combined to form different geometries of the constriction but we will focus on the combinations that are presented in Fig. 4. The height h_0 representing the smallest aperture in the channel (the throat of the glottis) can be varied from 0.1 mm to 5 mm using calibrated spacers (metal rings) in the block mounting. Pressures are measured at two positions: the first position is 8 mm upstream of the start of the constriction in the side wall of the cylindrical pipe (piezo electrical transducer PCB 116A with a Kistler charge amplifier type 5011) and the second position is in the throat of the constriction at the smallest aperture. A piezo resistive pressure transducer (Kulite XCS062) is mounted in the blocks using a pressure tap with a diameter of 0.4 mm, as is shown in Fig. 5.

The liplike round model is built with two half-cylinders with a radius of 10 mm. The pressure tap is exactly in the middle of the block. The vocal-fold models consist of a cylindrical part, followed by a linearly diverging part and another cylindrical part (Scherer and Titze, 1983). The angle of divergence α is either 20° or 10°, as shown in Fig. 4. These models are the same ones as used by Pelorson *et al.* (1994) and are based on the typical vocal-fold movement discussed in the Introduction (see Fig. 1). The diffuser angles are chosen in such a way that when $h_0 \approx 3$ mm with $\alpha = 10°$ the flow would be in the stable-diffuser-flow region and with $\alpha = 20°$ the flow would be outside the stable-diffuser-flow region, according to data on diffuser performance at high Reynolds numbers (Re of the order 10^5) (Blevins, 1984). For the lip-

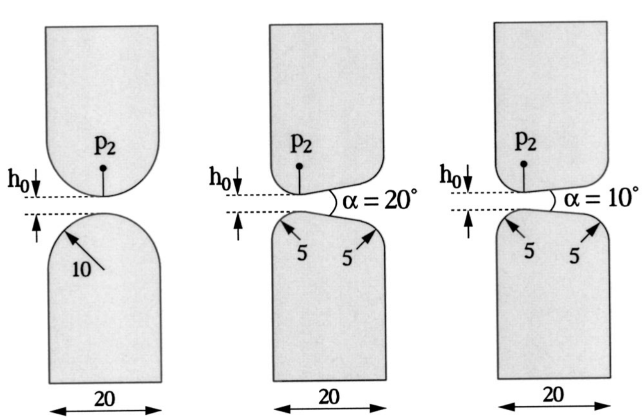

FIG. 4. Models that are studied: the model on the left is a liplike round model and the models on the right are diverging vocal-fold models. Measures are in millimeters. The arrows indicate the radii of curvature of the walls. The width of the blocks and hence the length of the glottal slit perpendicular to the flow direction is 30 mm.

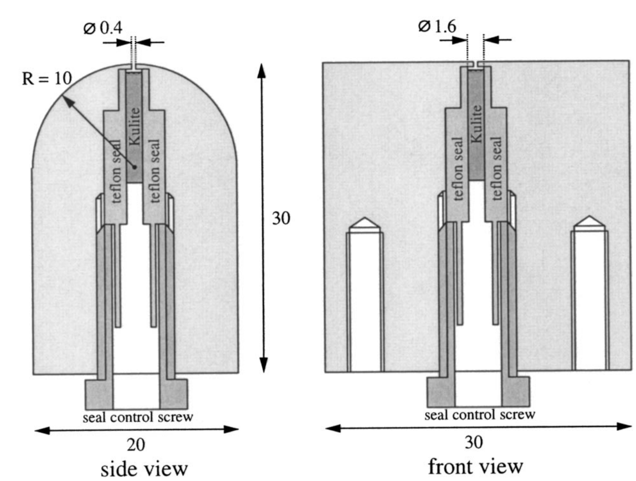

FIG. 5. Mounting of the Kulite pressure transducer in one of the brass blocks that form the constriction. A seal made of Teflon controlled by a screw is used to ensure a tight fit.

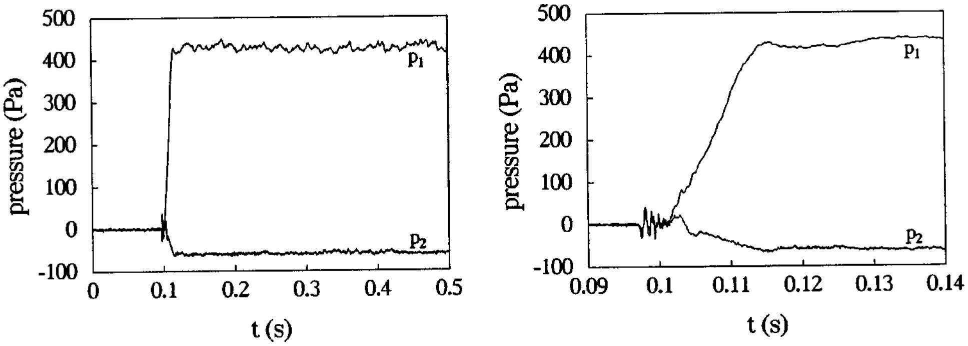

FIG. 6. Pressure measured in the pipe p_1 and in the throat p_2 for the liplike round geometry: $\Delta p = 430$ Pa and $h_0 = 0.99$ mm. The right graph is a close-up of the left graph, showing the transient behavior.

like model we will present in addition to the pressure data local velocity measurements obtained with a hot wire anemometer.

Using a laser detector system the opening of the valve is detected and the start of the measurement is triggered by this signal. During an experimental run pressures are measured and in some cases the velocity is measured simultaneously. The velocity is measured using a 4-μm-thick hot-wire in a constant-temperature anemometer. The signals are fed into a data acquisition system that is connected to a personal computer by means of a four-channel 12-bit ADC card (Keithley DAS-50). A typical experimental run lasts 500 ms while data are sampled at a frequency of 20 kHz.

In order to validate the accuracy of the pressure measurements, some experiments have been carried out using a straight channel with a smooth inlet and a sharp-edged outlet (Hofmans, 1998). Those tests confirmed the accuracy of the pressure measurements and the hot-wire anemometry, which was found to be of the order of 2%.

B. Results for the liplike round model

The liplike round model is studied for two reasons. First of all, the model can be considered a reference model for studying flow separation from a curved wall: because of the constant radius of curvature the separation point is usually not sensitive to external influences. The second reason is that this model is considered relevant for the study of the flow through the opening between the lips, which is important when considering plosives (Pelorson *et al.*, 1997) and brass instruments.

The experiments with the liplike models consist of pressure and velocity measurements. The pressure p_1 is measured in the pipe 8 mm upstream of the constriction while the pressure p_2 is measured at the smallest aperture (in the throat) of the constriction. The velocity is measured at various positions on the center line of the setup using the hot-wire anemometer. Experiments have been performed for two values of the throat height: $h_0 = 0.99$ mm and $h_0 = 3.36$ mm. It was found that the hot-wire probe disturbed the flow too much in the case of $h_0 = 0.99$ mm, so no velocity measurements have been done at the throat in this case. Since the results found for a throat height $h_0 = 0.99$ mm are very similar to results for $h_0 = 3.36$ mm, we mostly focus on results of the latter case.

In Fig. 6 a representative measurement is shown for the liplike models with a throat height $h_0 = 0.99$ mm. The final steady pressure drop Δp across the constriction is equal to 430 Pa. The opening time is approximately 15 ms, which, together with the length of the glottis model (20 mm) and the typical velocity $u_0 = \sqrt{2\Delta p/\rho}$, leads to a Strouhal number of 0.05. The Reynolds number is then approximately 1800 corresponding to loud speech. The left graph shows the pressure signals in the pipe p_1 upstream of the constriction and in the throat p_2 for a time range of 0.5 s. The right graph is a close-up of the left graph and shows the transient behavior in more detail in a time range of 0.05 s. The time axis is determined by the trigger for the measurement obtained by optical detection of the valve movement. In this and all subsequent graphs the trigger signal was generated at $t = 0.1$ s: by using the pretrigger capability of the ADC-card the measurement has already been recorded 0.1 s before the trigger is generated. The actual start of the flow is not determined since the optical detector setup is triggered by the valve movement and not by the flow, but it is reasonable to assume that this is close to the trigger point. In Fig. 7 two similar measurements with a throat height $h_0 = 3.36$ mm at a pressure drop of 290 Pa (Sr=0.05, Re=4900) and 690 Pa (Sr=0.03, Re=7600) are shown. Except for a few milliseconds before the trigger point the pressure in the pipe p_1 shows a smooth increase from zero to a steady value Δp. The small but distinct oscillations around the trigger point (at 0.1 s) are caused by the opening of the valve and could not be avoided in our setup. They also occur at zero pressure difference ($\Delta p = 0$). Hence we expect these oscillations to be due to acoustic waves generated by lateral movement of the valve before it actually opens. Using the optical detector setup the speed of the valve during opening is estimated to be in the range of 1.5 to 2 m/s. For an opening of 2 cm in the valve this corresponds to an opening time of the order of 10^{-2} s.

In Figs. 6 and 7 the pressure p_2 in the throat exhibits a particular behavior. The first few milliseconds of the experiments the pressure p_2 in the throat is rising proportionally to the pressure p_1 upstream of the glottis. This is due to the initial flow that is like a potential flow: boundary layers are still very thin and flow separation does not yet occur. The bulk flow is inviscid so velocity and pressure are related by Bernoulli's equation:

$$\rho \frac{\partial \phi_1}{\partial t} + \frac{1}{2}\rho u_1^2 + p_1 = \rho \frac{\partial \phi_2}{\partial t} + \frac{1}{2}\rho u_2^2 + p_2, \tag{1}$$

in which ρ is the density of air, u is the velocity, and ϕ is the velocity potential. The main contribution to the pressure drop

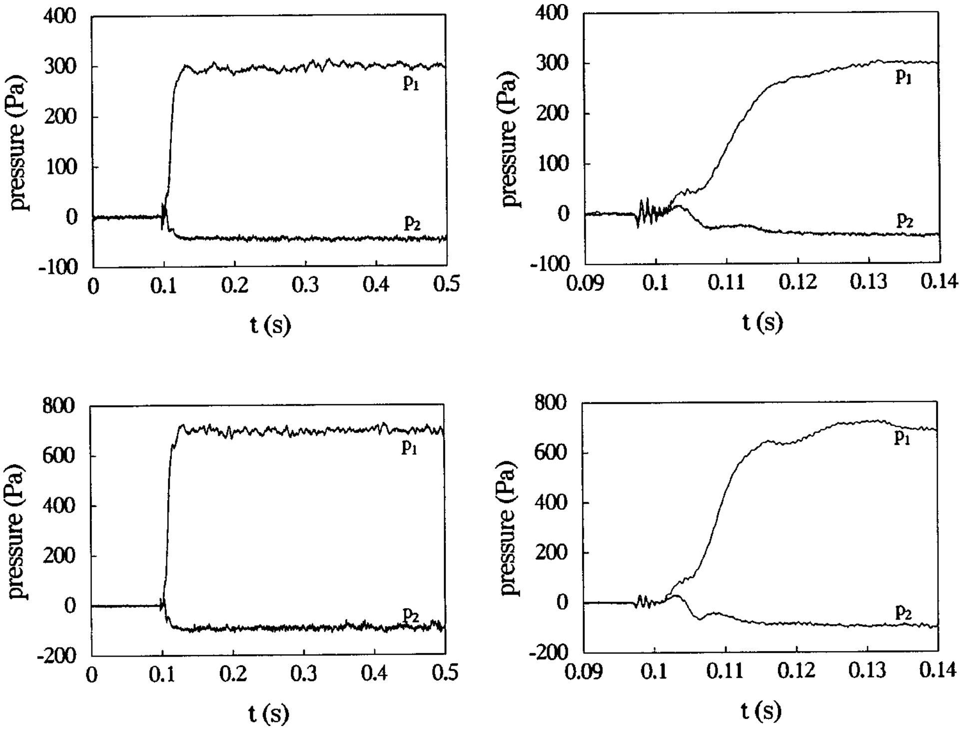

FIG. 7. Pressure measured in the pipe p_1 and in the throat p_2 for the liplike geometry: top graphs $\Delta p = 290$ Pa; bottom graphs $\Delta p = 690$ Pa, $h_0 = 3.36$ mm. The right graph is a close-up of the left graph, showing the transient behavior.

across the constriction is given by the inertial effects (the $1/2\rho u^2$-terms are negligible because the velocity is still very small). This implies that the pressure in the throat has a value that is somewhere between the pressure in the experiment room (by definition equal to zero) and the pressure in the pipe p_1. Typically p_2 is equal to 0.5 p_1 for the time interval $0.100\,\mathrm{s} < t < 0.105\,\mathrm{s}$, because the constriction is symmetric with respect to the throat and the main contribution to the inertial terms originates from this region. After the initial stage the flow separates from the walls of the constriction forming a jet. Finally, a steady situation is reached. If we assume the pressure in the jet to be equal to the pressure in the experiment room and if we assume the height of the jet h_s larger than the throat height h_0, then the pressure in the throat is lower than the pressure in the experiment room, since the velocity in the throat is higher than the velocity in the jet. This can be illustrated by inserting the one-dimensional equation of mass conservation $[u(x)h(x) = \Phi]$, thus neglecting boundary-layer effects, into the steady Bernoulli equation. Here $h(x)$ is the height of the channel and $\rho\Phi$ is the two-dimensional mass flux. This results in the following equation relating the pressure to the height of the channel:

$$\frac{p(x)}{\rho} + \frac{1}{2}\left(\frac{\Phi}{h(x)}\right)^2 = \frac{1}{2}\left(\frac{\Phi}{h_s}\right)^2, \tag{2}$$

in which h_s is the height of the channel at the separation point. By inserting p_1, pipe height h_p, p_2, and h_0 the following relationship between the pressure ratio p_2/p_1 and the various channel heights is obtained:

$$\frac{p_2}{p_1} = \frac{1-(h_s/h_0)^2}{1-(h_s/h_p)^2}, \tag{3}$$

which for $h_p \gg h_s$ reduces to

$$\frac{h_s}{h_0} = \sqrt{1 - \frac{p_2}{p_1}}. \tag{4}$$

Therefore the pressure in the throat would be an indication of the jet width h_s and consequently of the position of the separation point. As can be observed in Figs. 6 and 7, p_2 is indeed less than zero in the steady limit.

Although the experiments for both values of h_0 look very similar, a few small but distinct differences can be observed. The experiment with $h_0 = 3.36$ mm show an oscillatory behavior in the pressures p_1 and p_2 during the first milliseconds after the trigger point. This oscillation is less pronounced in the experiments with $h_0 = 0.99$ mm and has a lower frequency. Furthermore, the experiments with $h_0 = 0.99$ mm seem to reach the steady state in a more straightforward way. We expect that this behavior is related to an acoustical resonance of the pipe system, which is not fully damped by the sound absorbing material in the upstream pipe segment (see Fig. 3). A more narrow slit can be associated with larger acoustical dissipation. The oscillation frequency is of the order of magnitude of the lowest acoustical mode of an open pipe segment of the length of the main pipe.

By integrating Bernoulli's equation the velocity in the throat can be computed based on the pressure measurements p_1 and p_2. For this purpose Bernoulli's equation is rewritten in the following form:

$$\frac{\partial(\phi_2 - \phi_1)}{\partial t} = \frac{1}{2}(u_1^2 - u_2^2) + \frac{p_1 - p_2}{\rho}, \tag{5}$$

which, using the definition of ϕ, can be written as

$$L_{\mathrm{eff}}\frac{\partial u_2}{\partial t} = \frac{1}{2}(u_1^2 - u_2^2) + \frac{p_1 - p_2}{\rho}, \tag{6}$$

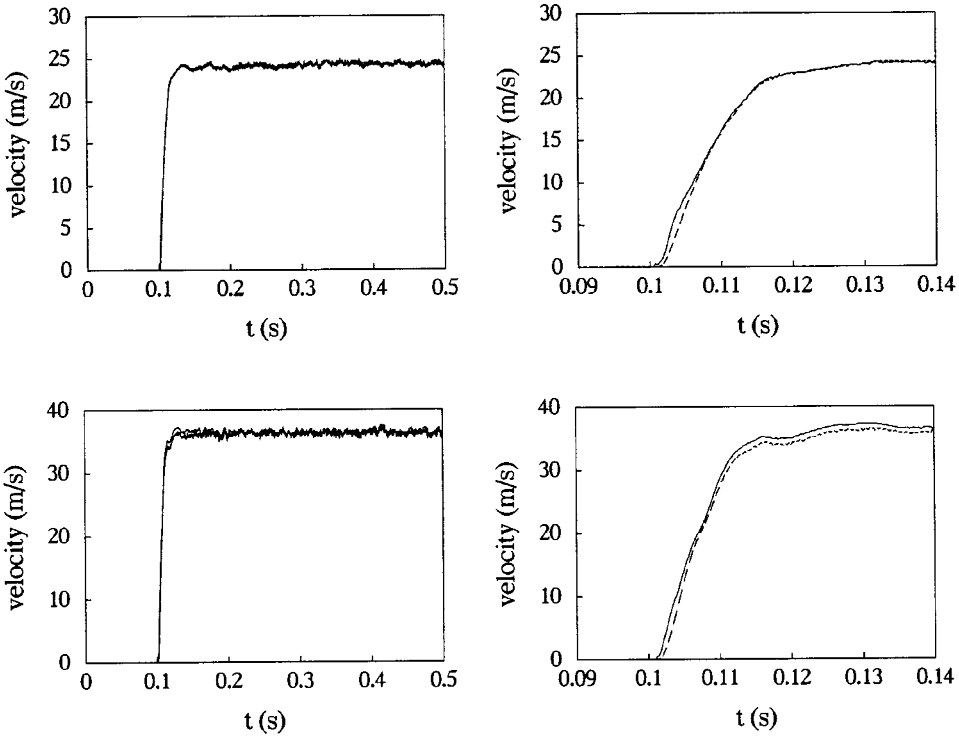

FIG. 8. Velocity measured in the throat (dashed line) and the velocity calculated in the throat by integration of the unsteady Bernoulli equation using the measured pressures p_1 and p_2 (solid line). Experiments performed on the liplike geometry: top graphs $\Delta p = 290$ Pa; bottom graphs $\Delta p = 690$ Pa, $h_0 = 3.36$ mm. The right graph is a close-up of the left graph, showing the transient behavior.

in which an effective length L_{eff} has been introduced. It is defined by

$$L_{\text{eff}} = \int_{x_1}^{x_2} \frac{h_0}{h(x)}\, dx, \tag{7}$$

where in the last step we assumed a uniform flow across the channel for any given x-position (quasi-one-dimensional flow).

In Fig. 8 the computed velocity (solid line) is compared to the velocity measured in the throat by means of the hot-wire anemometer (dashed line). The velocity that is computed is the velocity at the edge of the boundary layer, which does not have to agree with the velocity on the center line in a curved channel, because of the effect of curved streamlines on the pressure. It has been found, however, that this effect is considerably reduced in the throat because the boundary-layer growth in this region tends to cancel this effect. Furthermore, since flow separation takes place close to the throat, the curvature effect is also reduced (even neglecting boundary-layer growth). For this reason an assumption of uniform flow through the throat is quite reasonable. The pressure measurements of these experiments are shown in Fig. 7. A good overall agreement is found between hot-wire measurement and calculation of the velocity in the throat based on pressure measurements. This confirms the accuracy of the pressure measurements. However, in the initial stage of the experiments ($0.1 < t < 0.105$) the hot-wire measurements are delayed with respect to the computed velocity profiles, similar to the results found for the sharp edge nozzle configuration (Hofmans, 1998). This is expected to be due to a poor dynamical response of the hot-wire at low velocities.

Since one of the aims of this paper is to determine the validity of simplified models, results of the boundary-layer theory are compared to steady pressure measurements in the liplike models. The theoretical results are based on Pohlhausen's method (Pohlhausen, 1921) using a third-order polynomial to describe the velocity profile in the boundary layer and then solving the steady von Kármán equation as done previously by Pelorson *et al.* (1994). There are unfortunately some printing errors in the formulas provided by Pelorson *et al.* Correct formulas are provided in the Appendix. The steady pressures are measured by means of Betz water manometers with an accuracy of 0.05 mm H_2O ($\approx$0.5 Pa). Results are shown in Fig. 9. The markers represent measurements in the top and bottom walls of the constriction. The solid line represents the theoretical result.

The boundary-layer theory predicts a too high value of p_2/p_1. This might be the result of the assumptions that are made. In the theoretical model, the boundary layer is calculated up until the separation point. At the separation point the pressure is assumed to be equal to the external pressure (quasi-steady uniform velocity jet model). It is also possible to continue the boundary-layer calculation beyond the separation point. This leads to a lower prediction of p_2/p_1. However, these calculations do not converge to a constant pressure value as we increase the calculation domain and they are therefore not reliable. The third-order polynomial does not describe the flow accurately (far) beyond the separation point. These results may indicate that the assumption of constant pressure in the jet is not valid inside the constriction and that the reference point for the pressure in the boundary-layer model is not correctly chosen. Alternatively this might just be due to a poor prediction of the separation point by the boundary-layer model. This last hypothesis will be eliminated by comparison of boundary-layer theory with numerical calculations presented in Sec. III.

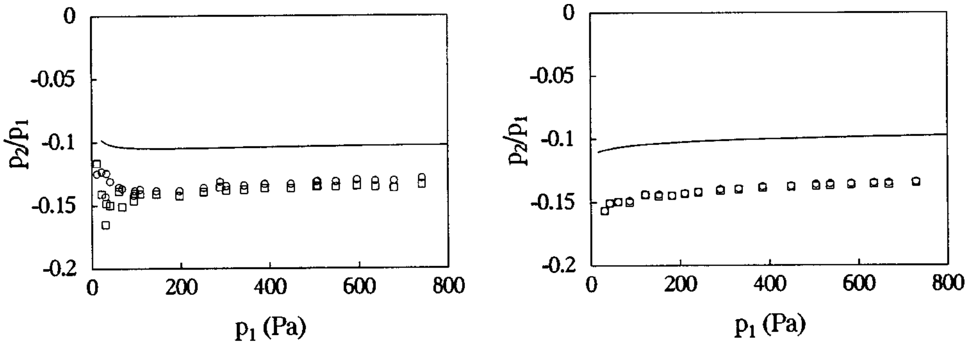

(a) $h_0 = 0.99$ mm (b) $h_0 = 3.36$ mm

FIG. 9. Comparing boundary-layer predictions (solid line) with steady pressure measurements at the throat in the top wall (○) and the bottom wall (□) of the liplike models.

C. Results for the 20°-diverging model

Models that are more specific for the study of the flow through the glottis are the two diverging scale models that are shown in Fig. 4. In this section we present results for the diffuser model with a total angle of divergence α of 20°. The flow through this model is investigated by means of unsteady pressure measurements at two positions: one in the pipe 8 mm upstream of the constriction and the other in the throat of the constriction. Measurements are done with two values for the height of the throat: $h_0 = 1.12$ mm and $h_0 = 3.50$ mm.

In Fig. 10 pressure measurements are presented for $h_0 = 1.12$ mm and two values of the steady pressure drop: $\Delta p = 301$ Pa ($\mathrm{Re} = 1.5 \times 10^3$) and $\Delta p = 627$ Pa ($\mathrm{Re} = 2 \times 10^3$). The right graphs show a close-up of the left graphs, focusing on the transient behavior. In fact each graph consists of two experimental results. Repeating the experiment several times we found that two distinctly different time histories for the pressure p_2 were obtained. As can be observed in Fig. 10, initially the two time histories collapse onto one curve and only after a certain time the two curves start to deviate, leading to two different steady-pressure values for p_2. This behavior is explained by an asymmetric flow due to the so-called Coanda effect (Tritton, 1988). The Coanda effect is due to viscous entrainment of the air that is caught between the jet and the walls of the channel. The symmetric jet becomes meta-stable and a small perturbation results in an adherence of the jet to either the top or bottom wall of the channel. Since this phenomenon can be triggered by a small asymmetry in the flow, both states are possible in a symmetric setup. The pressure signal p_1 is very similar to the signals found in the liplike model. Also the initial increase in p_2—corresponding to an unsteady potential flow—can be observed in this case. However, here the similarities with the results of the liplike model end and a different behavior of p_2 is observed. Note the rather strong downward peak in p_2 just before the steady limit is reached.

In Fig. 11 equivalent pressure measurements are presented for $h_0 = 3.50$ mm and two values of the steady pressure drop: $\Delta p = 268$ Pa ($\mathrm{Re} = 4 \times 10^3$) and $\Delta p = 528$ Pa (Re

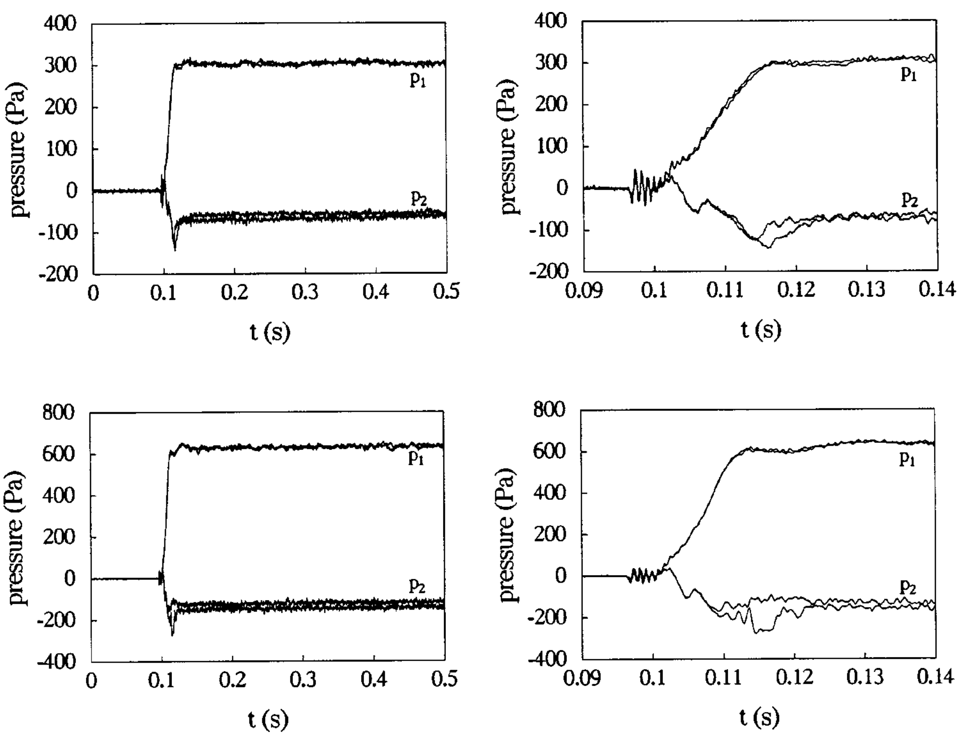

FIG. 10. Pressure measured in the pipe p_1 and in the throat p_2 for the diffuser geometry with $\alpha = 20°$: top graphs $\Delta p = 301$ Pa; bottom graphs $\Delta p = 627$ Pa, $h_0 = 1.12$ mm. The right graph is a close-up of the left graph, showing the transient behavior. In each graph two experimental runs are shown.

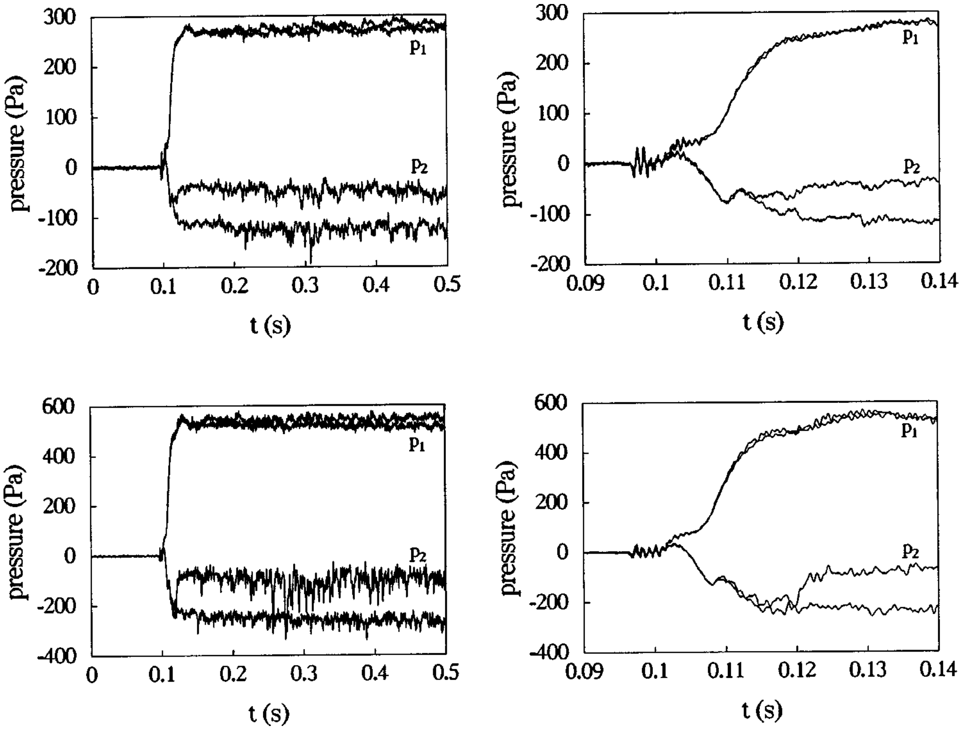

FIG. 11. Pressure measured in the pipe p_1 and in the throat p_2 for the diffuser geometry with $\alpha=20°$: top graphs $\Delta p=268$ Pa; bottom graphs $\Delta p=528$ Pa, $h_0=3.50$ mm. The right graph is a close-up of the left graph, showing the transient behavior. In each graph two experimental runs are shown.

$=6\times10^3$). The Coanda effect is also observed in this configuration and the behavior is very similar to the previous case, except that the bifurcation of the two states is much more prominent. The presence of the Coanda effect was confirmed by flow visualizations and by simultaneous measurements at both sides of the throat using less accurate pressure transducers. Pelorson and Hirschberg (1997) also presented accurate simultaneous pressure measurements that confirm the occurrence of a Coanda effect. Note also the increased level of the fluctuations on the pressure signals which might indicate the onset of turbulent flow. In general it was found that the flow was very unstable in this configuration.

Both Figs. 10 and 11 illustrate the fact that the establishment of the Coanda effect takes time. In order to quantify this claim, the time at which the two time histories of p_2 start to deviate is measured as a function of the steady pressure drop. The time is taken with respect to the trigger point, since this is a good indication of the actual start of the flow. The results are presented in Fig. 12. Similar results have been presented by Pelorson and Hirschberg (1997). The results for $h_0=1.12$ mm seem to exhibit a linear relationship with the pressure drop, although data at low pressures ($p_1<300$ Pa, $\mathrm{Re}<1.5\times10^3$) are lacking. On the other hand, the results for $h_0=3.50$ mm do not exhibit this and in fact for a large range of p_1 ($250\,\mathrm{Pa}<p_1<700\,\mathrm{Pa}$, $4\times10^3<\mathrm{Re}<8\times10^3$) the transition time remains unchanged at approximately 13 ms (translated to physiological conditions 1.5 ms). Below 250 Pa the transition time increases strongly to 25 ms (translated to physiological conditions 2.8 ms). The transient in our glottis model lasts approximately 20 ms, while the related closing or opening time of the glottis oscillation is approximately 2 ms for typical male voiced sound production at 100 Hz (see Fig. 2). So the significance of the Coanda effect is not yet clearly established. On the other hand, in the real glottis the movement of the walls is an important factor and the consequences of this movement for the Coanda effect are yet to be determined but could be quite significant. In the closing phase of the glottis, the Coanda effect is expected to be reduced because the wall movement is equivalent to an injection of fluid at the wall. The opposite occurs

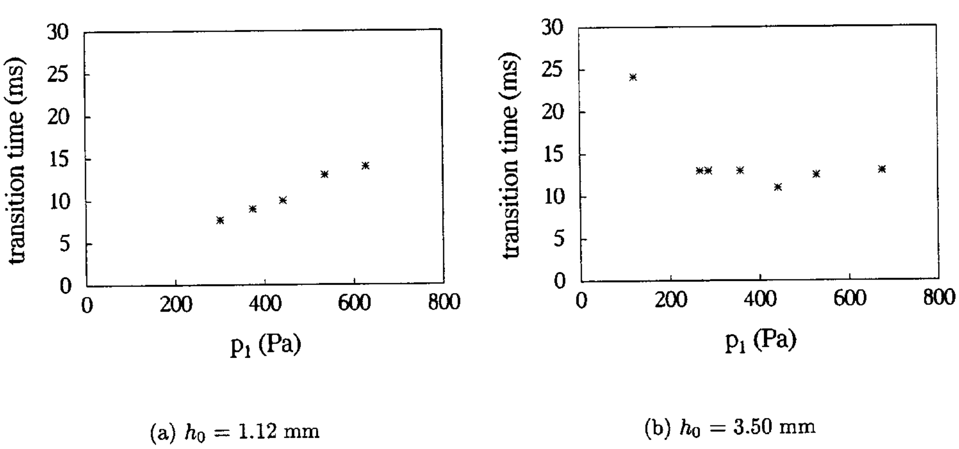

FIG. 12. The time with respect to the trigger point at 0.1 s at which the flow starts to exhibit two states due to the Coanda effect for the diffuser model with $\alpha=20°$.

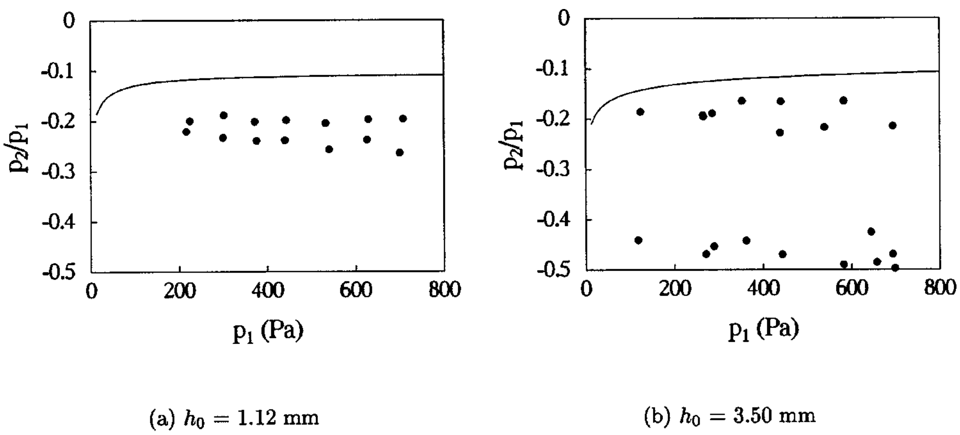

FIG. 13. Comparing boundary-layer predictions (solid line) with steady limit pressures obtained from the unsteady experiments (markers): vocal-fold model with α=20°.

during the opening phase. However, in the opening phase the glottis is convergent and the Coanda effect is expected to be only a minor effect.

In order to compare the experimental results with predictions of the boundary-layer theory, the steady pressure ratio p_2/p_1 is determined in the unsteady experiments. The theoretical results are again based on Pohlhausen's method (Pohlhausen, 1921) using a third-order polynomial to describe the velocity profile in the boundary layer. Results are shown in Fig. 13. For each value of p_1 two values of p_2 are found experimentally. The different values are due to the adherence of the flow to either the upper wall of the constriction that contains the pressure tap (lower results) or to the opposite wall (upper results). For $h_0 = 1.12$ mm the two sets of values differ by 25%, while for $h_0 = 3.50$ mm they differ by a factor of 2. Again the theoretical prediction results in a too high value of p_2 (i.e., not negative enough), although a comparison is not completely justified due to the assumption of a symmetric solution in the theoretical boundary-layer model. Similar to the results found in the liplike model, an increase in the pressure downstream of the separation point is neglected. Because of the asymmetry of the flow, no conclusions on the point of separation can be drawn based on the pressure measurements.

D. Results for the 10°-diverging model

In this section we present results for the diffuser model with a total angle of divergence α of 10°. The flow through this model is again investigated by means of unsteady pressure measurements at two positions: one in the pipe 8 mm upstream of the constriction and the other in the throat of the constriction. Measurements are done with two values for the height of the throat: $h_0 = 1.01$ mm and $h_0 = 3.39$ mm.

In Fig. 14 pressure measurements are presented for $h_0 = 1.01$ mm and three values of the steady pressure drop: $\Delta p = 224$ Pa (Re$=1.2\times 10^3$), $\Delta p = 432$ Pa (Re$=1.8\times 10^3$), and $\Delta p = 682$ Pa (Re$=2.1\times 10^3$). The right graphs show a close-up of the left graphs, focusing on the transient behavior. The pressure signal p_1 is very similar to the signals found in the previous two scale models. Also the initial increase in p_2 can be observed in this case. However, again here the similarities with previous results end and different behavior of p_2 is observed. With increasing pressure an increasing level of fluctuations can be observed in p_2. Especially large fluctuations are observed for $\Delta p = 682$ Pa. This behavior is similar to the behavior observed in the 20°-diverging model with $h_0 = 3.50$ mm. However, p_1 is much more stable in this case and only one value is found for p_2. This behavior is apparently not due to the Coanda effect and simultaneous pressure measurements at both sides of the glottis displayed symmetric behavior (Pelorson *et al.*, 1995). A possible explanation is a shift of the very unstable separation point due to the transition from laminar flow to turbulent flow. Turbulence enhances strongly the flow entrainment by the jet, thus creating a low pressure region between the wall and the jet downstream of the separation point which pushes the separation point downstream. This is a symmetrical effect which occurs at both sides of the jet. This effect is even more prominent in the results obtained with $h_0 = 3.39$ mm as presented in Fig. 15. Three sets of pressure measurements are presented for $\Delta p = 161$ Pa (Re$=3\times 10^3$), 407 Pa (Re$=5\times 10^3$), and 654 Pa (Re$=6\times 10^3$). The top and center graphs show a distinctive, abrupt transition from a temporary stable solution to a new stable solution, while in the bottom graph this transition is already occurring during the initial transient. The difference in the level of the fluctuations before and after the transition indicates a transition from a laminar jet flow to a turbulent jet flow. The jet turbulence is indeed clearly observed in the flow visualizations (Pelorson *et al.*, 1994). Since a turbulent jet has a much stronger entrainment than a laminar flow, the net effect is to delay separation until the end of the diffuser when the diffuser angle is small. This would result in a much lower value for p_2. In fact we will show that the glottis model is acting like a well-designed diffuser for this configuration when turbulence has appeared in the jet flow. This behavior also agrees with the data presented in Blevins (1984) at much higher Reynolds numbers (Re of the order 10^5).

In Fig. 16 the steady pressure limits are compared to the theoretical prediction based on Pohlhausen's method (Pohlhausen, 1921) using a third-order polynomial to describe the velocity profile in the laminar boundary layers. In the case $h_0 = 1.01$ mm no abrupt transition is observed and therefore only one set of values is plotted in the left graph of Fig. 16. For low values of p_1 the agreement with the boundary-layer prediction is reasonable. An increasing deviation from the boundary-layer prediction is found with increasing value of p_1. In the case $h_0 = 3.39$ mm, a distinctive abrupt transition

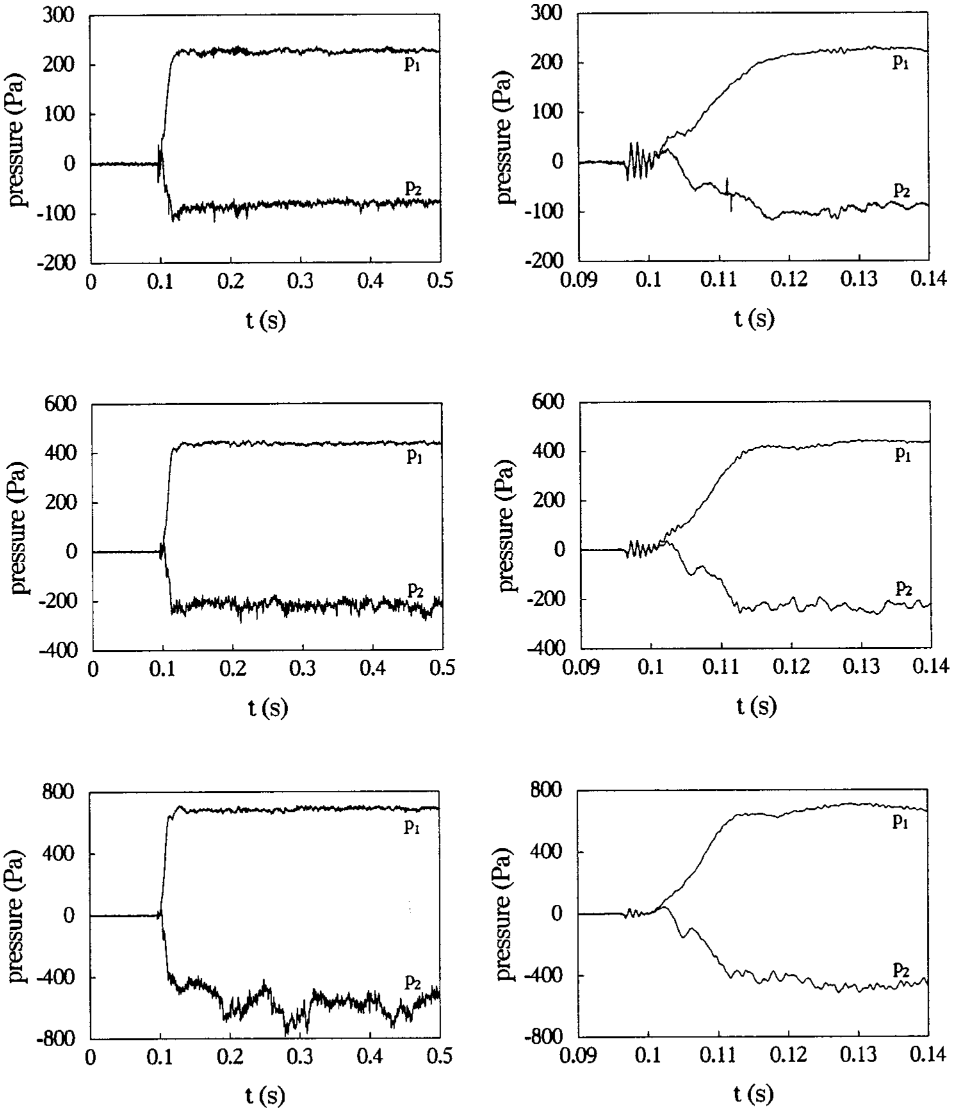

FIG. 14. Pressure measured in the pipe p_1 and in the throat p_2 for the diffuser geometry with $\alpha=10°$: top graphs $\Delta p=224$ Pa; center graphs $\Delta p=432$ Pa; bottom graphs $\Delta p=682$ Pa, $h_0=1.01$ mm. The right graph is a close-up of the left graph, showing the transient behavior.

is found for low values of p_1. In that case, two values for p_2 can be determined, one value before the transition and one value after the transition. For higher values of p_1 the transition occurs too early, so that it is not possible to determine a stable laminar value for p_2 before the transition. The values of p_2 before the transition at low values of p_1 agree quite well with the theoretical prediction. The turbulent results p_2 of course do not agree with the prediction of the laminar boundary-layer theory.

Using Eq. (4) the height h_s at the separation point can be estimated from the pressure ratio. In Fig. 17 the results are plotted. Clearly visible is the shift of the separation point in the downstream direction due to turbulence. This means that the flow remains a further distance attached to the walls of the glottis model as the pressure difference in the experiments increases. For $h_0=3.39$ mm a limit is reached above $p_1=200$ Pa (Re=4500). The limit $h_s/h_0\approx1.55$ in the right graph of Fig. 17 coincides with the value of h/h_0 at the end of the linearly diverging part of the constriction. In that case we do not expect a significant pressure recovery in the free jet.

In Fig. 18 the moment at which the transition occurs is plotted as a function of the pressure drop p_1 across the constriction. This figure illustrates that like the Coanda effect, turbulence needs a long time before it is established. For a typical Reynolds number relevant in speech ($\mathrm{Re}_h=3000$), the time delay in our experiments is 100 ms which corresponds to 11 ms under physiological conditions. For normal male voiced sound the oscillation period is of the order of 10 ms (see Fig. 2) which corresponds to 6 ms open phase. So, similar to the Coanda effect, in a pulselike flow with a duration of the order of 10 ms this effect might not be important in normal speech. However, Fig. 15 shows that at high pressures, corresponding to shouting, the pressure in the throat of the glottis never reaches a steady laminar value before turbulence sets in completely. It is further expected that such effects are sensitive to the movement of the walls and hence this can induce a hysteresis in the flow separation behavior as a function of h_0.

III. NUMERICAL SIMULATION

A. Method

The incompressible two-dimensional Navier–Stokes equations are solved using the so-called viscous vortex-blob

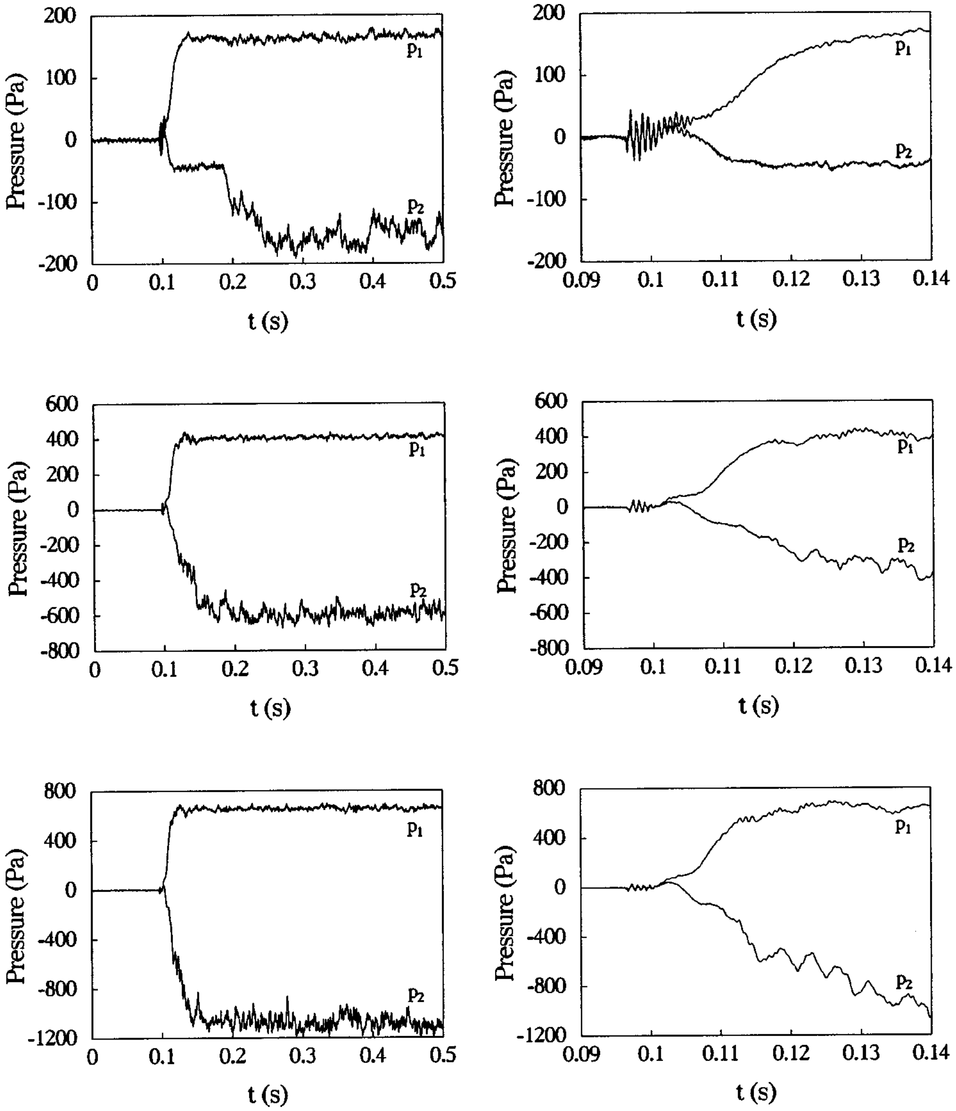

FIG. 15. As in Fig. 14, with $\alpha=10°$: top graphs $\Delta p=161$ Pa; center graphs $\Delta p=407$ Pa; bottom graphs $\Delta p=654$ Pa, $h_0=3.39$ mm.

method (Graziani *et al.*, 1995; Ranucci, 1995). The method is based on a desingularized point vortex method. The solution is obtained in the form of the vorticity distribution ω by solving the vorticity-transport equation:

$$\frac{\partial\omega}{\partial t}+\mathbf{u}\cdot\nabla\omega=\frac{1}{\mathrm{Re}}\nabla^2\omega, \tag{8}$$

where $\mathbf{u}$ is the local velocity field and Re is the Reynolds number. For an appropriate treatment of both the convective and the diffusive time scale as well as for the accurate approximation of the nonlinear term, the equation has been split into a "Euler step" and a "Stokes step" according to the Chorin–Marsden product formula (Chorin *et al.*, 1978). The first step is governed by the inviscid-flow equation stating

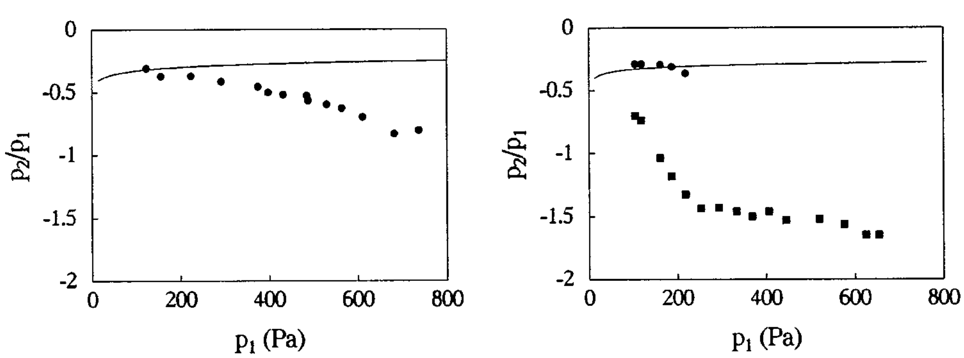

(a) $h_0 = 1.01$ mm

(b) $h_0 = 3.39$ mm

FIG. 16. Comparing boundary-layer predictions (solid line) with steady limit pressures obtained from the unsteady experiments: ● before transition; ■ after transition. No transition occurred in the experiments with $h_0=1.01$ mm. Diffuser model with $\alpha=10°$.

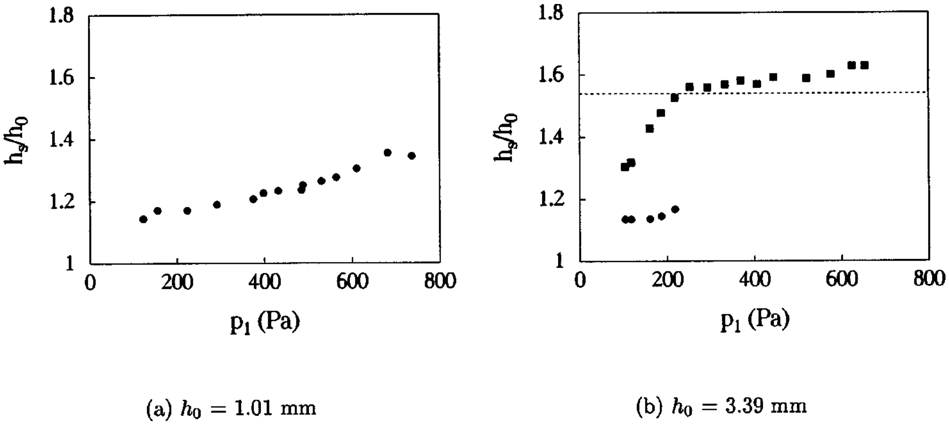

FIG. 17. The ratio of the channel height at the separation point and the throat height h_s/h_0 as computed from p_2/p_1 using Eq. (4): ● before transition; ■ after transition. The dashed line represent the height at the end of the linearly diverging section. Diffuser model with $\alpha = 10°$.

that the material identity of the vortical particles is advected by the velocity field:

$$\frac{D\omega}{Dt} = 0. \tag{9}$$

In the second step, Stokes' equation in vorticity form in two dimensions becomes

$$\frac{\partial \omega}{\partial t} = \frac{1}{\mathrm{Re}} \nabla^2 \omega. \tag{10}$$

The fractional-step scheme provides the most appropriate and convenient solution for each substep. The vorticity field defined on the computational body-fitted grid with mesh size h is approximated as

$$\omega(\mathbf{x}, t^n) = \sum_{j=1}^{N} \Gamma(\mathbf{x}_j, t^n)\, \delta(\mathbf{x} - \mathbf{x}_j), \tag{11}$$

where $\Gamma(\mathbf{x}_j, t_n) = \omega(\mathbf{x}_j, t_n) h^2$ is the circulation at the grid point $\mathbf{x}_j$ and time t_n and $\delta(\mathbf{x} - \mathbf{x}_j)$ is the Dirac delta function. Since the interaction between two point vortices diverges as the point vortices approach each other, a desingularization of this interaction is appropriate as has been first discussed by Chorin and Bernard (1973) and later by others such as Beale and Majda (1985). In our method the point-vortex interaction is desingularized by the higher-order kernel of Lucquin-Descreux (1987). Further details on the numerical method can be found in Hofmans (1998).

B. Input for the simulations

Using the viscous vortex-blob method, four simulations have been done with the diverging vocal-fold models at moderate Reynolds number (of the order 10^3): $\alpha = 20°$, $h_0 = 1.05$ mm, and $h_0 = 3.35$ mm; $\alpha = 10°$, $h_0 = 1.05$ mm, and $h_0 = 3.35$ mm. The numerical method yields a solution of the two-dimensional incompressible Navier–Stokes equations and needs an imposed inflow velocity (u_{in}) as input. The steady-state value of the inflow velocity is used as the reference velocity u_{ref}. This input is obtained from experimental pressure measurements (as presented in the previous paragraphs). First a ninth-order polynomial is fitted to the pressure difference $(p_1 - p_2)$ between pipe and throat as a function of time. Next this smooth fitted pressure profile is integrated in time using the unsteady Bernoulli equation to find the inflow velocity as a function of time. This method is more practical than a polynomial fit to the velocity profile because this usually requires at least two separate fits. In Fig. 19 an example is shown of the result of this procedure. In the left graph the pressure difference $(p_1 - p_2)$ is plotted together with the fitted polynomial. In the right graph the resulting scaled inflow velocity is plotted as a function of time. Time equal to 0 is defined to be the start of the simulation.

The computational domain for the diffuser models is shown in Fig. 20. The inflow-velocity (u_{in}) is uniformly imposed on the left inflow boundary. The height of the inflow channel is related to the radius of curvature r and the throat height h_0. It is defined as the reference length l_{ref} in the simulation $l_{\mathrm{ref}} = 4r + h_0$. On the right the outflow boundary is a far-field semi-circular domain (at a distance of 27 l_{ref}). On this boundary a radial outflow is assumed and the outflow velocity is determined from the inflow velocity by the continuity equation. Since the geometry that we are interested in is symmetric with respect to its center line, the computation is restricted to the upper half of the domain, hence the use of a symmetry line as a lower boundary and only half a glottis as the upper boundary. This also reduces the computational time and memory requirements by approximately a factor of 2. The boundary is discretized by a set of panels. A densification of panels is applied in the region around the glottis and on the symmetry line. A typical run requires 1600 to 1900 panels to build the geometry and uses 50 000 to 100 000 point vortices to discretize the vorticity field. The region in which the full (viscous) Navier–Stokes equations are solved is restricted to the viscous domain. Outside this

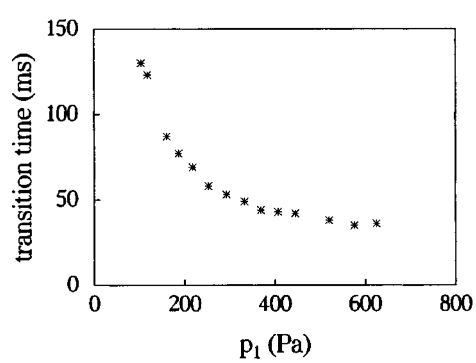

FIG. 18. The time with respect to the trigger point at 0.1 s at which the flow starts to change significantly due to the onset of turbulence. Diffuser model with $\alpha = 10°$.

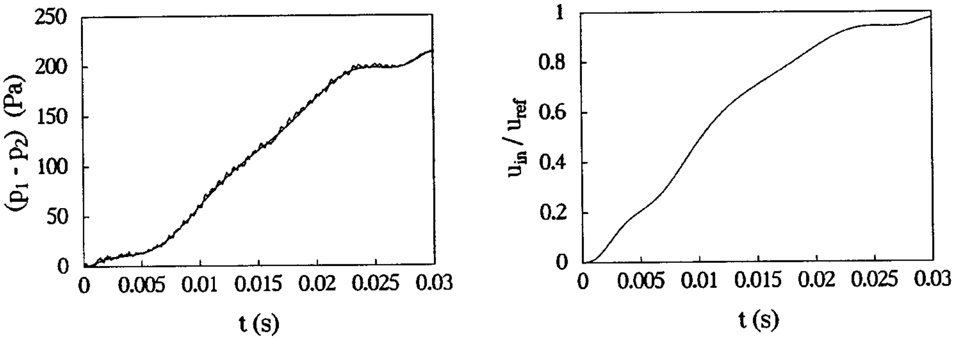

FIG. 19. Input for a numerical simulation. The scaled inflow $u_{\mathrm{in}}/u_{\mathrm{ref}}$ (right graph) for the numerical simulation is obtained from the pressure difference (p_1-p_2) (left graph) by fitting a ninth-order polynomial (left graph) and integrating the unsteady Bernoulli equation, steady-state inflow velocity $u_{\mathrm{ref}}=2.609$ m/s.

domain only the inviscid Euler equations are solved. The viscous domain includes the whole jet-region and the region of flow separation (which is in fact the whole constriction area). In the inflow domain and in the upper region of the outflow channel viscous effects are neglected since they have negligible influence on the results.

C. Results

The inflow boundary condition has been obtained from experimentally measured pressure differences (p_1-p_2) in the four geometries. The experimental pressures are shown in Fig. 21 represented by the thin lines. The pressure p_1 was measured 8 mm upstream of the constriction while the pressure p_2 was measured in the throat of the constriction. Also shown are the numerical results for p_1 and p_2 by means of the thick lines. Although the experimental pressure difference (p_1-p_2) was used to determine the inflow velocity, this does not impose individual values of either p_1 or p_2. The results in Fig. 21 demonstrate that the numerical method yields very reasonable results for the pressures p_1 and p_2. Note that the very unstable behavior that was found experimentally for the case $\alpha=20°$ and $h_0=3.50$ mm (see Fig. 11) seems also to be present in the numerical result for $\alpha=20°$ and $h_0=3.35$ mm, shown in the top right graph of Fig. 21. An explanation for this unstable behavior is suggested by a close-up of the numerical vorticity in the diffuser region of the glottis shown in Fig. 22. As these plots show, the interaction between the jet and the walls of the diffuser is very complex. After 0.02 s, bursts of vorticity leave the walls at regular intervals in time. Oscillatory pressure fluctuations in experiments could well be associated with this behavior.

In order to study the behavior of the separation point in these flows, the calculated height h_s of the channel at the separation point is plotted versus time in Fig. 23. As references, the heights that are associated with the starting point and the end point of the linear divergent part of the diffuser section are indicated by the dashed horizontal lines. The definition of a separation point is not obvious in an unsteady flow. We used the definition of the separation point for steady flows: $\partial u/\partial y=0$ on the wall, which is equivalent to $\omega_{\mathrm{wall}}=0$. This choice was made because it makes a comparison to a quasi-steady boundary-layer model straightforward.

The behavior visible in the top two graphs for $\alpha=20°$ is very different from that in the bottom two graphs for $\alpha=10°$. First of all, for $\alpha=20°$ flow separation starts somewhere halfway in the constriction and moves very rapidly to the throat of the constriction. A steady value just downstream of the constriction on the cylindrical part is reached after 10 ms. In the $\alpha=10°$ case, flow separation starts at the end of the constriction on the cylindrical part. It then moves rapidly to a stable point somewhere on the diffuser part of the vocal-fold model. The model is acting like a diffuser with marginal flow separation [also called stall (Blevins, 1984)], and a small perturbation can have a significant influence on the separation point. The sensitivity of the separation point to small perturbations observed in those laminar simulations support the hypothesis that a transition from a laminar to a turbulent flow results in a sudden change of the position of the sepa-

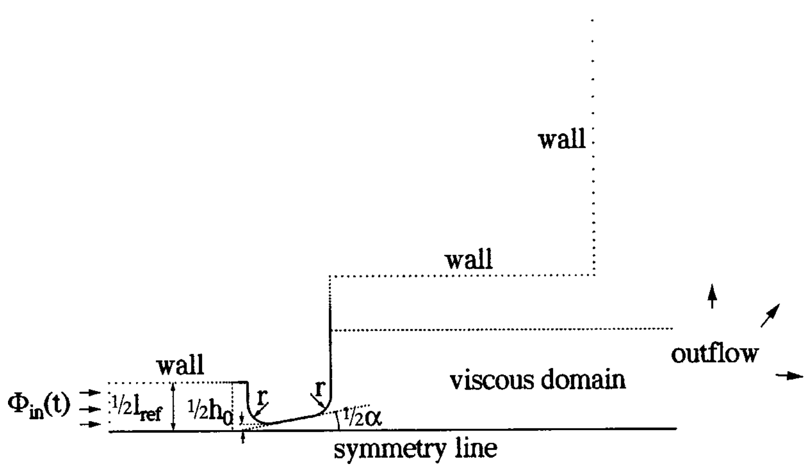

FIG. 20. Two-dimensional domain used in the numerical simulations. Throat height h_0 and total angle of divergence α are input parameters. The inflow channel has a total height of $4r+h_0$.

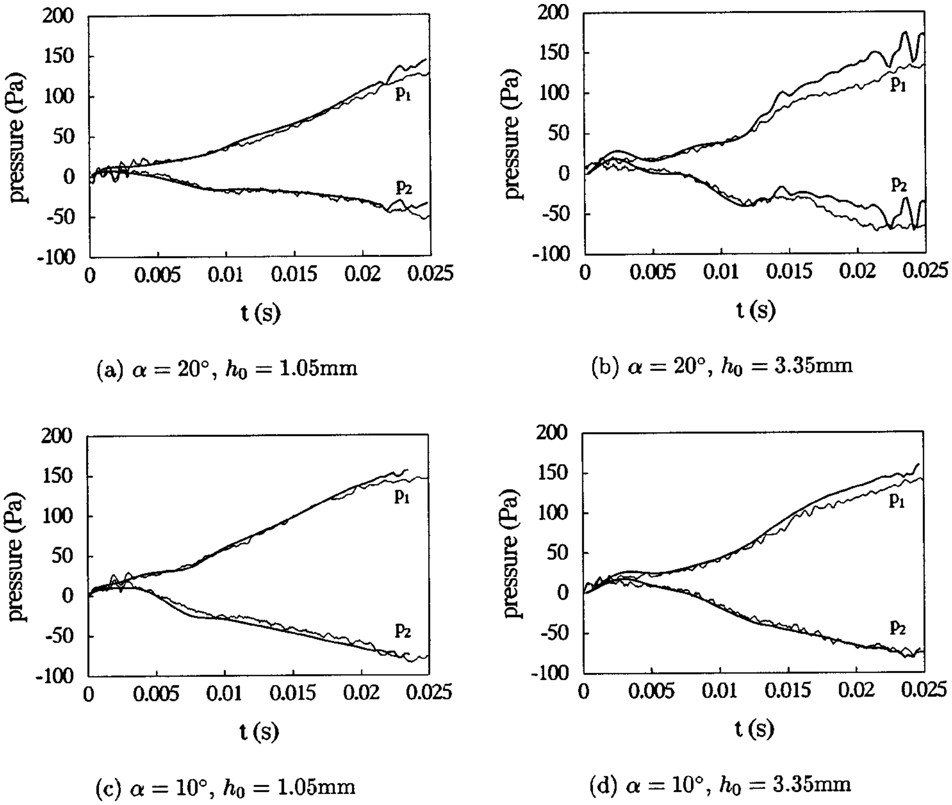

FIG. 21. Comparing numerical results for the pressures p_1 and p_2 (thick lines) to the experimental pressures (thin lines) from which the respective inflow velocities have been obtained.

ration point and of the pressure in the throat as observed in the experiments presented in Fig. 15.

After having demonstrated the complexity of this type of flow we will evaluate a simplified quasi-steady description of the flow. In Fig. 24 a close-up of the flow through the glottis is presented. The figure shows the velocity profiles in the region of the throat and illustrates the fact that a boundary-layer description is reasonable in the region around the throat. The velocity profiles exhibit a thin boundary layer near the walls and an approximately uniform profile in the bulk of the flow. Only further downstream the first large vortical structures can be observed.

Similar to Figs. 13 and 16 we present in Fig. 25 the pressure ratio $(p_2-p_s)/(p_1-p_s)$ as a function of $(p_1$

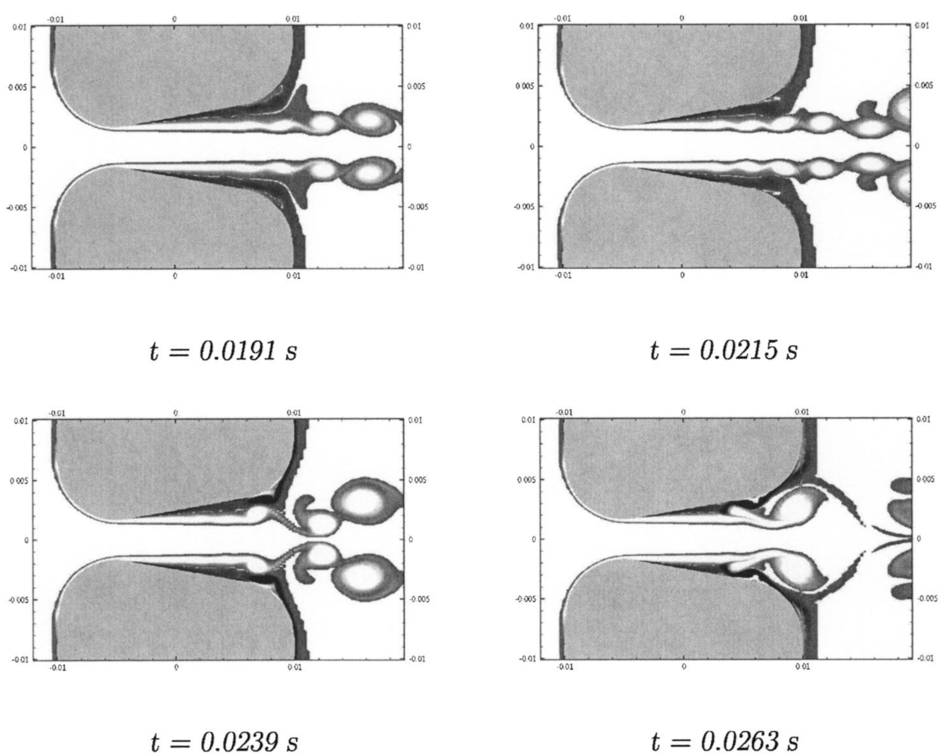

FIG. 22. Close-up of vorticity distribution in the diffuser region showing a complex interaction of vortices and the diffuser walls. Results obtained for α=20° and h_0=3.35 mm.

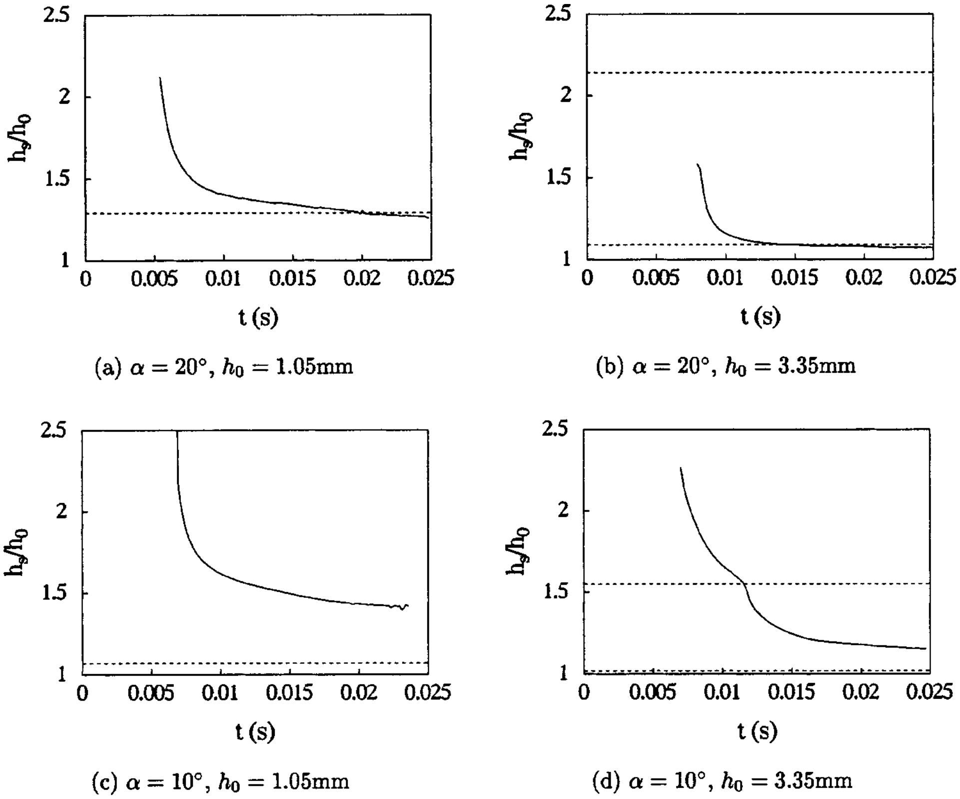

FIG. 23. Point of zero wall stress (as defined by $\omega_{\mathrm{wall}}=0$ on the wall) as a function of time obtained from the numerical simulations. The dashed lines illustrate the starting point (lower line) and the end point (upper line) of the diffuser section. This upper line is out of the range in the left graphs for $h_0 = 1.05$ mm as it corresponds to $h_s/h_0 = 7$.

$-p_s$), remembering that p_1, p_2, and p_s can be functions of time. Although the boundary-layer model incorporates the assumption that the pressure at the separation point is equal to zero ($p_s=0$), this is not the case in the numerical simulations. The separation point in the numerical results is determined using the condition $\omega_{\mathrm{wall}}=0$ (see Fig. 23). Then p_s is the pressure on the symmetry line at the horizontal (stream-wise) position of the separation point. Hence the ratio $(p_2-p_s)/(p_1-p_s)$ can be determined from the numerical results.

After an initial stage, in which the flow is essentially unsteady, we see that the agreement between numerical results and boundary-layer prediction is quite good. This is surprising since the boundary-layer prediction and the steady limit of the experiments did not agree so well (see Figs. 13 and 16). An explanation can be found in Fig. 26. In this figure the pressures p_1 and p_2 are plotted together with (p_1-p_s) and (p_2-p_s) in each graph. The dashed lines represent the pressure with respect to the far field, which agreed with the experimentally measured pressure as illustrated by Fig. 21. The solid smooth lines represent the pressure with respect to the separation point, as used in Fig. 25. The difference between these two lines is the contribution to the pressure due to the flow downstream of the separation point inside the constriction and to the jet flow. Note that the pressure drop p_2 from throat to separation point is about equal to the pressure drop from the separation point to the far-field. This conclusion is in agreement with the results obtained recently by Scherer *et al.* (2001) by means of steady flow numerical solution of the Navier–Stokes equations. This explains the large discrepancies found between experiments and boundary-layer theory. Note also that the pressure fluctuations are due to the flow downstream of the separation point. This indicates that the structure of the jet flow might be important to predict the source of sound in speech modeling. In particular, the jet instabilities can induce higher frequencies which are experienced in speech as broadband "noise."

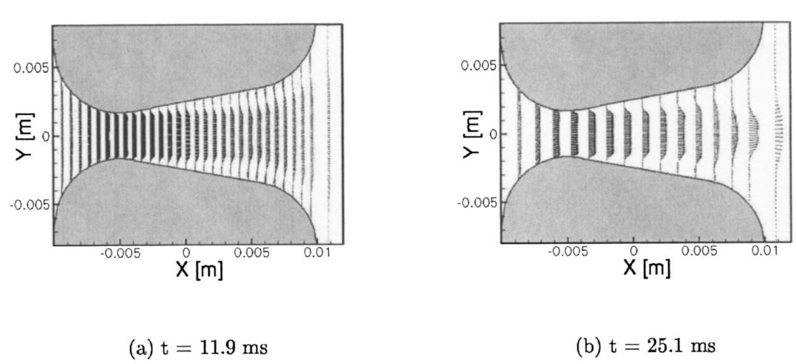

FIG. 24. Close-up of the constriction region showing the velocity vectors. α=20° and h_0=3.35 mm.

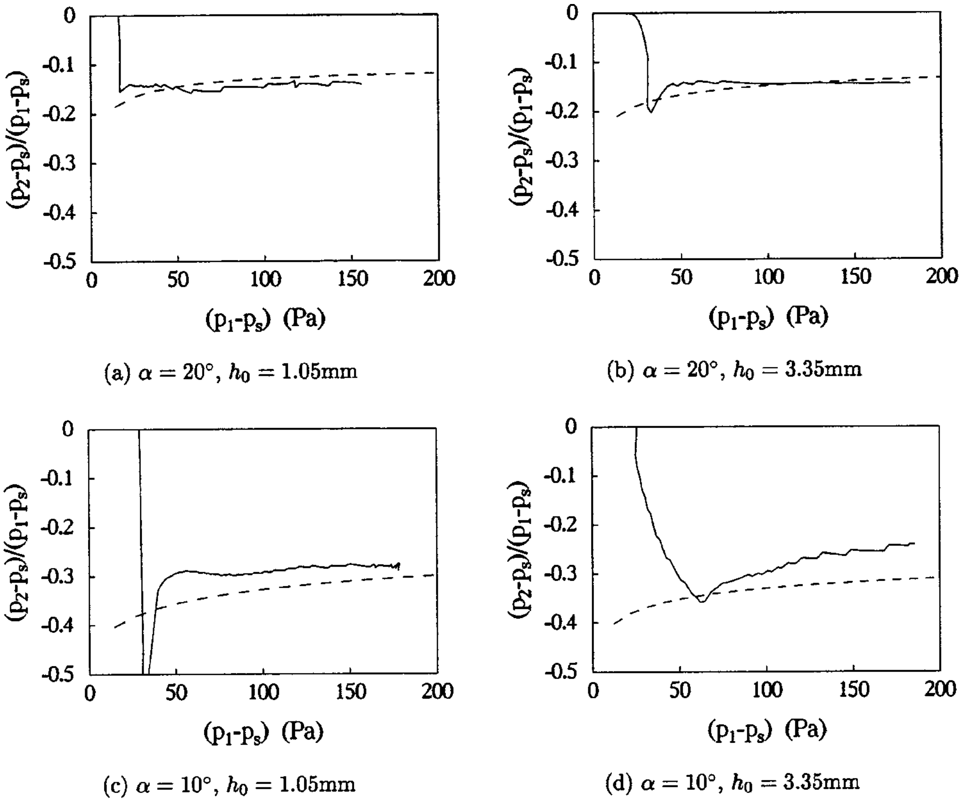

FIG. 25. Comparing numerical results (solid lines) for the pressure ratio $(p_2-p_s)/(p_1-p_s)$ to quasi-steady boundary-layer predictions (dashed lines). p_s is the pressure at the point of zero wall stress.

IV. CONCLUDING REMARKS

In this paper we set out to describe the flow through *in vitro* models of the glottis. By means of a combined experimental, numerical, and theoretical study we have managed to explain most of what was observed.

First of all, the richness of phenomena observed in the experiments demonstrates the complexity of this type of flow. However, we have shown results that make it reasonable to ignore some of these phenomena in a model of the flow through the glottis. The Coanda effect as well as the transition to a turbulent flow need in order to appear a time delay comparable to the opening or closing time of the glot-

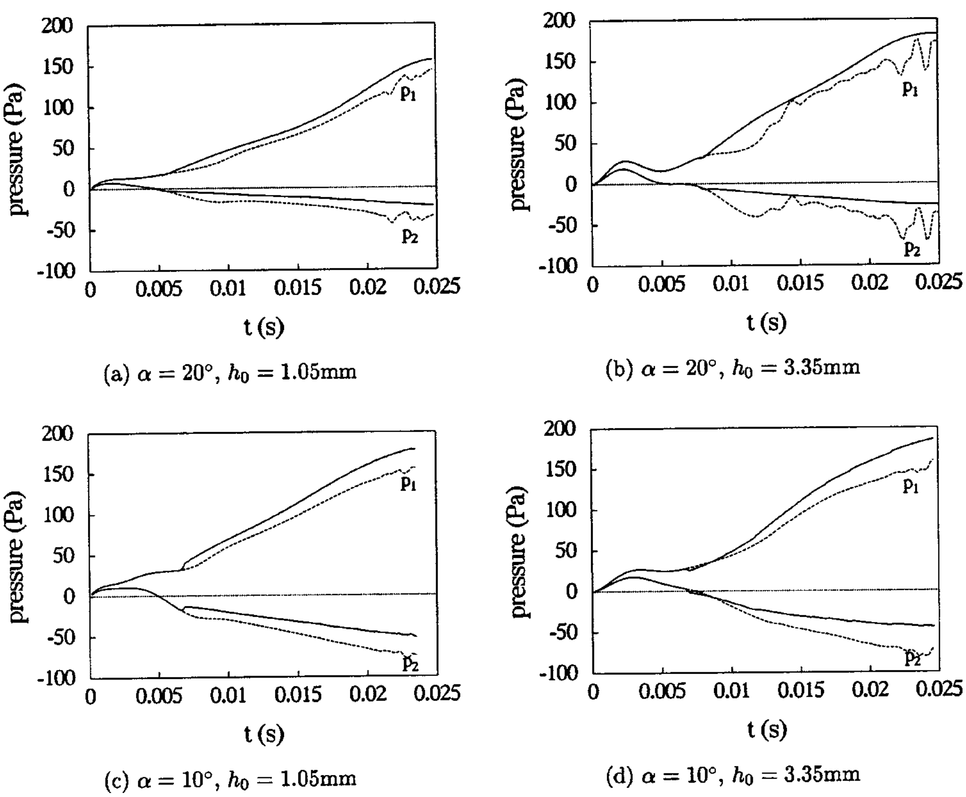

FIG. 26. Influence of the jet on the pressure signal. Solid lines represent pressures (p_1-p_s) and (p_2-p_s) with respect to the pressure at point of zero wall stress, while the dashed lines represent pressures p_1 and p_2 with respect to the far-field pressure as used in the experiments.

tis in normal male speech production. Female speech production corresponds to typical frequencies of 200 Hz and would be even less sensitive to these effects. This conclusion is drawn, however, for rigid models of the glottis with an unsteady flow at relatively high Reynolds numbers compared to normal speech conditions.

The behavior of the diffuserlike vocal-fold models at a Reynolds number of the order 10^3 seems similar to what has been reported in literature about diffuser performance at much higher Reynolds number of the order 10^5. Similar to results reported by Kwong and Dowling (1994) obtained in a diffuser, we found experimentally and numerically that the vocal-fold model with a diffuser angle of 20° and an initial height $h_0 = 3.50$ mm exhibited very unsteady flow behavior. For the vocal-fold model with a diffuser angle of 10° and an initial height $h_0 = 3.39$ mm we found experimentally that it acts as a well-designed diffuser. This behavior is conform data on diffuser performance (Blevins, 1984).

The comparison between experiment and boundary-layer theory in combination with a quasi-steady free jet indicated that the theoretical boundary-layer model showed typical systematic errors of 30% in the throat pressure. The numerical study, on the other hand, confirmed that the boundary-layer model was not inadequate but that some of the assumptions had to be adjusted. After an initial period of essentially unsteady flow the quasi-steady laminar boundary-layer model predicts the position of the separation point with a surprising accuracy. However, the assumption of a uniform pressure in the jet is inadequate. This is confirmed by considering that the difference between the far-field pressure and pressure at the separation point is almost as large as the pressure difference between the pressure at the separation point and the pressure at the throat of the glottis. This implies that the pressure difference due to the jet is significant. This is in agreement with the steady flow calculations of Scherer *et al.* (2001). The assumption of a quasi-steady jet without pressure recovery (quasi-parallel flow implying a uniform pressure) is in fact the main source of inaccuracy in our prediction of the throat pressure. An improvement of the jet model is necessary. Such an improvement, however, is only relevant when the mechanical modelling of the vocal folds has a similar degree of sophistication (Lous *et al.*, 1998).

Numerical results obtained by means of the vortex blob method can predict the flow inside the glottis. However, downstream of the flow separation point, turbulence appears which drastically changes the character of the flow, making the numerical results useless. This effect is suppressed by flow acceleration in the attack transient but is expected to be dramatic in the deceleration phase (Hofmans, 1998).

While this paper was being revised, experiments with oscillating walls have been performed by Deverge *et al.* (2002) which globally confirm the validity of our results.

ACKNOWLEDGMENTS

Part of this research was sponsored by the Dutch Technology Foundation (Project No. ETN33.2952).

APPENDIX: POHLHAUSEN'S METHOD

Analogous to Pohlhausen (1921), we have used a third-order polynomial description of the velocity profile in the boundary layer $u(x,y)$:

$$u(x,y) = U(x) \sum_{i=0}^{3} a_i \left(\frac{y}{\delta}\right)^i,$$

in which $U(x)$ is the main flow velocity at the edge of the boundary layer, y is the coordinate perpendicular to the wall, δ is the boundary-layer thickness, and a_i are the coefficients which are functions of the coordinate x along the wall. In order to determine the coefficients the polynomial has to satisfy four boundary conditions:

$$u(x,0) = 0, \quad u(x,\delta) = U,$$

$$\left.\frac{\partial u}{\partial y}\right|_{y=\delta} = 0, \quad \nu \left.\frac{\partial^2 u}{\partial y^2}\right|_{y=0} = -U \frac{dU}{dx}.$$

Upon substitution of the polynomial in the boundary conditions the coefficients a_i are determined. Introducing the parameter $\Lambda = (\delta^2/\nu)(\mathrm{d}U/\mathrm{d}x)$ the coefficients are

$$a_0 = 0, \quad a_1 = \frac{\Lambda}{4} + \frac{3}{2}, \quad a_2 = -\frac{\Lambda}{2}, \quad a_3 = \frac{\Lambda}{4} - \frac{1}{2}.$$

Alipour, F., Fan, C., and Scherer, R. C. (**1996**). "A numerical simulation of laryngeal flow in a forced-oscillation glottal model," J. Comput. Speech Language **10**, 75–93.

Alipour, F., and Titze, I. R. (**1996**). "Combined simulation of two-dimensional airflow and vocal fold vibration," in *Vocal Fold Physiology: Controlling Complexity and Chaos*, edited by P. J. Davis and N. H. Fletcher (Singular, San Diego), pp. 17–29.

Beale, J. T., and Majda, A. (**1985**). "High order accurate vortex methods with explicit velocity kernels," J. Comput. Phys. **58**, 188–208.

Blevins, R. D. (**1984**). *Applied Fluid Dynamics Handbook* (Van Nostrand Reinhold, New York).

Cancelli, C., and Pedley, T. J. (**1985**). "A separated-flow model for collapsible tube oscillations," J. Fluid Mech. **157**, 375–404.

Chorin, A. L., and Bernard, P. S. (**1973**). "Discretization of a vortex sheet, with an example of roll-up," J. Comput. Phys. **13**, 423–429.

Chorin, A. J., Hughes, T. J. R., McCracken, M. F., and Marsden, J. E. (**1978**). "Product formulas and numerical algorithms," Commun. Pure Appl. Math. **31**, 205–256.

Deverge, M., Pelorson, X., Vilain, C., Lagrée, P.-Y., Chentouf, F., Willems, J., and Hirschberg, A. (**2002**). "Influence of the collision on the flow through in-vitro rigid models of the vocal folds," submitted for publication.

De Vries, M. (**2000**). "A voice for the voiceless," Ph.D. thesis, Rijksuniversiteit Groningen, Groningen.

Graziani, G., Ranucci, M., and Piva, R. (**1995**). "From a boundary integral formulation to a vortex method for viscous flows," Comput. Mech. **15**, 301–314.

Hirschberg, A., Pelorson, X., Hofmans, G. C. J., Van Hassel, R. R., and Wijnands, A. P. J. (**1996**). "Starting transient of the flow through an in-vitro model of the vocal folds," in *Vocal Fold Physiology: Controlling Complexity and Chaos*, edited by P. J. Davis and N. H. Fletcher (Singular, San Diego), pp. 31–46.

Hofmans, G. C. J. (**1998**). "Vortex sound in confined flows," Ph.D. thesis, Eindhoven University of Technology, Eindhoven.

Ishizaka, K., and Flanagan, J. L. (**1972**). "Synthesis of voiced sounds from a two-mass model of the vocal cords," Bell Syst. Tech. J. **51**, 1233–1268.

Kwong, A. H. M., and Dowling, A. P. (**1994**). "Unsteady flow in diffusers," ASME J. Fluids Eng. **116**, 842–847.

Liljencrants, J. (**1993**). Private communication.

Lous, N. J. C., Hofmans, G. C. J., Veldhuis, R. N. J., and Hirschberg, A. (**1998**). ''A symmetrical two-mass vocal-fold model coupled to vocal tract and trachea, with application to prosthesis design,'' Acta Acoust. **84**, 1135–1150.

Lucquin-Descreux, B. (**1987**). ''Particle approximation of the two-dimensional Navier-Stokes equations,'' Rech. Aérosp. **4**, 1–12.

Luo, X. Y., and Pedley, T. J. (**1996**). ''A numerical simulation of unsteady flow in a two-dimensional collapsible channel,'' J. Fluid Mech. **314**, 191–225.

Pedley, T. J., and Luo, X. Y. (**1998**). ''Modeling flow and oscillations in collapsible tubes,'' Theor. Comput. Fluid Dyn. **10**, 277–294.

Pedrizzetti, G. (**1996**). ''Unsteady tube flow over an expansion,'' J. Fluid Mech. **310**, 89–111.

Pelorson, X., and Hirschberg, A. (**1997**). ''*In vitro* study of the glottal and supra-glottal flow during phonation,'' in *Proceedings of the 4th Congress on Acoustics, Marseille*, Teknea, Toulouse, pp. 337–340.

Pelorson, X., Hirschberg, A., Van Hassel, R. R., Wijnands, A. P. J., and Auregan, Y. (**1994**). ''Theoretical and experimental study of quasi-steady flow separation within the glottis during phonation. Application to a modified two-mass model,'' J. Acoust. Soc. Am. **96**, 3416–3431.

Pelorson, X., Hirschberg, A., Wijnands, A. P. J., and Bailliet, H. (**1995**). ''Description of the flow through *in-vitro* models of the glottis during phonation,'' Acta Acoust. **96**, 3416–3431.

Pelorson, X., Hofmans, G. C. J., Ranucci, M., and Bosch, R. C. M. (**1997**). ''On the fluid mechanics of bilabial plosives,'' Speech Commun. **22**, 155–172.

Pohlhausen, K. (**1921**). ''Zur Näherungsweisen Integration der Differentialgleichung der laminaren Reibungsschicht,'' Z. Angew. Math. Mech. **1**, 252–268.

Ranucci, M. (**1995**). ''Effetti del rilascio di vorticitá nell'interazione corpo-fluido,'' Ph.D. thesis, University of Rome ''La Sapienza,'' Rome.

Rosenfeld, M. (**1995**). ''A numerical study of pulsating flow behind a constriction,'' J. Fluid Mech. **301**, 203–223.

Rothenberg, M. (**1981**). ''Acoustic interaction between the glottal source and vocal tract,'' in *Proceedings of the Kurume Vocal Fold Physiology Conference*, edited by K. N. Stevens and N. Hirano (Univ. of Tokyo, Tokyo), pp. 305–328.

Scherer, R. C., Shinwari, D., De Witt, K. J., Zhang, C., Kucinschi, B. R., and Afjeh, A. A. (**2001**). ''Intraglottal pressure profiles for a symmetric and oblique glottis with an divergence angle of 10 degrees,'' J. Acoust. Soc. Am. **109**, 1616–1630.

Scherer, R. C., and Titze, I. R. (**1983**). ''Pressure-flow relationship in a model of the laryngeal airway with diverging glottis,'' *Vocal Fold Physiology: Contemporary Research and Clinical Issues*, edited by D. M. Bless and J. H. Abbs (College Hill, San Diego), pp. 177–193.

Tritton, D. J. (**1988**). *Physical Fluid Dynamics* (Clarendon, Oxford).